Available online at www.sciencedirect.com
ScienceDirect
Journal of Catalysis 254 (2008) 365–373
JOURNAL OF CATALYSIS
www.elsevier.com/locate/jcat

Visible light-induced partial oxidation of cyclohexane on hydrophobically modified chromium-containing mesoporous silica with molecular oxygen

Yasuhiro Shiraishi *, Hiroshi Ohara, Takayuki Hirai

Research Center for Solar Energy Chemistry, and Division of Chemical Engineering, Graduate School of Engineering Science, Osaka University, Toyonaka 560-8531, Japan

Received 21 November 2007; revised 13 January 2008; accepted 14 January 2008

Available online 7 February 2008

Abstract

Photocatalytic oxidation of neat cyclohexane (CHA) with molecular oxygen was carried out using hydrophobically modified Cr-containing mesoporous silica under visible light. Two catalysts (Cr/MOS and Cr/MOS-cal) containing highly dispersed chromate species were synthesized by Cr impregnation onto mesoporous organosilica (MOS) prepared with tetraethyl orthosilicate (TEOS) and 1,2-bis(triethoxysilyl)ethane (BTESE). Cr/MOS was synthesized by Cr impregnation onto MOS followed by calcination, and Cr/MOS-cal was synthesized by calcination of MOS, Cr impregnation, and calcination. Both catalysts promoted partial CHA oxidation with high selectivity (>86%). Cr/MOS-cal synthesized with 10% BTESE showed the highest catalytic activity, due mainly to the higher surface hydrophobicity, which accelerated access of CHA to the chromate species. ESR analysis revealed that the tetrahedrally coordinated chromate species (T_d^{6+}) on Cr/MOS-cal were photoexcited and formed highly reduced T_d^{4+*} species with high catalytic activity. This also contributed to the high catalytic activity of Cr/MOS-cal.

Keywords: Visible light; Photocatalyst; Partial oxidation; Cyclohexane; Cr-containing mesoporous silica

1. Introduction

Interest is increasing in the partial oxidation of cyclohexane (CHA) to cyclohexanol (CHA-ol) and cyclohexanone (CHA-one), because these products are the important intermediates in ε-caprolactam synthesis [1,2]. Partial CHA oxidation with molecular oxygen (O_2) in heterogeneous catalytic systems has attracted much attention [3,4]. Photocatalytic CHA oxidation in liquid/solid heterogeneous systems also has been studied extensively with various catalysts, including TiO_2 [5–12], Fe porphyrin-modified TiO_2 [13,14], polyoxotungstate-modified SiO_2 [15], and V_2O_5-impregnated Al_2O_3 [16,17]. These systems require UV light for catalyst activation and have low oxidation selectivity. In previous work, we found that Cr-containing silica with highly dispersed chromate species catalyzed highly selective partial CHA oxidation (>97%) in an acetonitrile/catalyst heterogeneous system under visible light ($\lambda > 400$ nm) [18,19]. This photocatalytic system has the highest selectivity for partial CHA oxidation among the systems proposed to date.

For practical applications, the reaction should be performed under solvent-free conditions. However, as described herein, when used in a solvent-free system, the catalyst shows very low activity, with a turnover number (TON) for the formation of partially oxidized (PO) products [= (amount of CHA-one and CHA-ol formed)/(amount of Cr on the catalyst)] of only 0.8 (5 h). Consequently, improving the catalytic activity is necessary.

The rate of heterogeneous catalytic reactions depends strongly on the surface hydrophobicity of catalysts, because the "affinity" of a reactant with a catalytically active site depends on the surface properties [20,21]. Mesoporous silicas, such as MCM-41, are hydrophilic because of their large quantity of surface silanol groups [22], whereas CHA is hydrophobic. Thus, the rate of CHA oxidation would be improved by increasing the surface hydrophobicity of the catalyst. The surface of the mesoporous silica can easily be made hydrophobic by introducing hydrophobic organic fragments. The mesoporous organosil-

* Corresponding author. Fax: +81 6 6850 6273.
E-mail address: shiraish@cheng.es.osaka-u.ac.jp (Y. Shiraishi).

0021-9517/$ – see front matter
doi:10.1016/j.jcat.2008.01.016

ica (MOS) can be synthesized by two methods, postsynthesis [23,24] and direct synthesis [25–27]. The former is based on the reaction of mesoporous silica with organochloro- or organoalkoxysilanes, where the organic fragments are anchored on the silica surface. The latter is based on simultaneous hydrolysis of tetraethyl orthosilicate (TEOS) and organoalkoxysilanes [e.g., 1,2-bis(triethoxysilyl)ethane (BTESE)] with surfactant. In the latter method, organic fragments are homogeneously introduced into the silica framework, and larger quantities of organic fragments are incorporated than in the former method. The obtained MOSs have high surface areas and well-ordered mesostructures. In addition, the surface hydrophobicity of MOS is easily controlled by changing the TEOS and BTESE compositions. Another notable feature is that MOS retains high surface hydrophobicity after calcination, even though the organic fragments are removed [28].

In the present work, we synthesized Cr-containing MOS catalysts and used them in the photocatalytic oxidation of CHA under solvent-free conditions. We expected to find enhanced access of CHA to the photoexcited chromate species on the hydrophobic catalyst surface. Two types of catalysts with highly dispersed chromate species, Cr/MOS and Cr/MOS-cal, were synthesized. Cr/MOS was synthesized by Cr impregnation onto MOS followed by calcination, whereas Cr/MOS-cal was synthesized by calcination of MOS, Cr impregnation, and calcination. Eight different Cr/MOS(x) and Cr/MOS-cal(x) catalysts with different BTESE compositions [x (mol%) = BTESE/(BTESE + TEOS) × 100; $x = 5$, 10, 20, and 50] were synthesized. The effects of organic modification on the catalytic activity and oxidation selectivity were compared with those of Cr/MCM-41 prepared only with TEOS. We found that the Cr/MOS(10)-cal catalyst had threefold higher activity than the Cr/MCM-41 catalyst while maintaining high selectivity. We also carried out an ESR analysis to clarify the properties of the photoexcited chromate species. We found that the catalytic activity of Cr-containing MOS depends strongly on the surface hydrophobicity, pore structure, and active site structure, which in turn are strongly affected by the amount of BTESE present and the synthesis procedure used.

2. Experimental

2.1. Materials

All of the reagents used were of the highest commercial quality, supplied by Wako, Tokyo Kasei, and Sigma–Aldrich and used without further purification. Water was purified by the Milli Q system. The MCM-41 and MOS(x) supports [$x = 5$, 10, 20, and 50] and the Cr/MCM-41, Cr/MOS(x), and Cr/MOS(x)-cal catalysts were synthesized as described in the following sections.

2.1.1. MCM-41

The MCM-41 was synthesized as described previously [29]. TEOS (100 mmol, 20.8 g) was added to 2-propanol (82 g) containing hexadecyltrimethylammonium bromide (C_{16}TMABr; 27.3 g) and stirred at room temperature. Then 5 ml of 2-propanol was added to a tetramethylammonium hydroxide solution (TMAOH, 15 wt% aqueous solution, 4.24 g). The resulting solution was added to the aforementioned mixture and stirred at room temperature for 24 h. A TMAOH solution (11.6 g) and water (138 g) were added dropwise to the mixture and stirred for 1 h at room temperature. The resulting mixture was stirred at 358 K for 4 h to evaporate the 2-propanol. The resulting gel was transferred into a Teflon bottle and settled for 11 days at 373 K. The resulting solid was recovered by filtration, washed with water and ethanol, and dried at 333 K in vacuo. The solid thus obtained was calcined at 813 K under air flow for 6 h.

2.1.2. MOS(x) [$x = 5$, 10, 20, and 50]

These supports were synthesized as described previously [30]. In a typical synthesis for $x = 10$, C_{16}TMABr (5.47 g) was added to 32 g of water. Then TEOS (45 mmol, 9.36 g) and BTESE (5 mmol, 1.84 g) were added to the solution. A TMAOH solution (15 wt% aqueous solution, 4.56 g) was added to the resulting mixture and stirred at room temperature for 36 h. The precipitate thus formed was recovered by filtration and washed with water. The resulting solid was redispersed in an alkaline solution (pH 10.5, 32 g) containing C_{16}TMABr (5.47 g) and settled at 358–363 K for 12 h. The resulting MOS(x) was recovered by filtration, washed with water and ethanol, and dried in vacuo at room temperature.

2.1.3. Catalysts

Cr/MCM-41 and Cr/MOS(x) were synthesized as follows: MCM-41 or MOS(x) support (2 g) was stirred in water (100 ml) containing $Cr(NO_3)_3{\cdot}9H_2O$ (4 mg) at 353 K for 12 h, with evaporation of water. The yellowish powder thus obtained was calcined at 773 K under air flow for 5 h. Cr/MOS(x)-cal was synthesized as follows: MOS(x) was calcined at 773 K under air flow for 4 h to yield a MOS(x)-cal support. Cr impregnation followed by calcination was carried out in a manner similar to that for Cr/MCM-41 and Cr/MOS(x) to yield a Cr/MOS(x)-cal catalyst.

2.2. Photoreaction procedure

Each catalyst (50 mg) was added to CHA (10 ml) in a Pyrex glass tube (20 cm^3, ⌀ 10 mm), and each tube was sealed with a rubber septum cap. O_2 was bubbled through the solution for 5 min at 273 K to prevent the evaporation of CHA. The sample was photoirradiated by a Xe lamp (2 kW; Ushio Inc.) filtered through an aqueous $NaNO_2$ (3 wt%) solution to give light wavelengths of $\lambda > 400$ nm. The temperature of the solution during photoirradiation was 313 K. The light intensity was 16.0 mW m^{-2} at 400–530 nm (through the filter). After photoirradiation, the gas-phase product was analyzed by GC-TCD (Shimadzu GC-8A). The resulting solution was recovered by centrifugation, and the catalyst was washed thoroughly with MeCN (10 ml). The combined solution was analyzed by GC-FID (Shimadzu GC-1700).

Table 1
Properties of supports

Support	S_{BET}[a] ($m^2\ g^{-1}$)	V_p[b] ($mm^3\ g^{-1}$)	D_p[c] (nm)	a_0[d] (nm)	T_w[e] (nm)	V_m[f] (mmol g^{-1})	q_{CHA}[g] (molecules nm^{-2})
MCM-41	1070	1092	2.6	4.4	2.4	1.89	1.06
MOS(5)	920	1159	3.2	5.0	2.7	2.07	1.35
MOS(10)	887	1213	3.7	5.7	2.9	2.65	1.80
MOS(20)	942	1238	3.7	6.4	3.6	2.06	1.32
MOS(50)	838	1265	4.3	6.9	3.6	2.06	1.48
MOS(5)-cal	1010	1219	3.1	4.8	2.4	1.67	1.00
MOS(10)-cal	933	1499	2.9	5.5	3.6	2.79	1.80
MOS(20)-cal	786	1081	3.7	5.9	3.1	1.79	1.37
MOS(50)-cal	639	831	3.7	6.1	3.3	1.53	1.39

[a] BET surface area determined by N_2 adsorption–desorption data (see Supplementary material, Fig. S2).
[b] Pore volume.
[c] Average pore diameter.
[d] Lattice constant determined by XRD (see Supplementary material, Fig. S1).
[e] Wall thickness $= a_0 \times 2/3^{1/2} - D_p$.
[f] Total adsorption capacity of CHA at $p/p_0 = 0.80$ determined by CHA adsorption data.
[g] CHA adsorption capacity per unit surface area $= V_m/10^3 \times 10^{-18}/S_{BET} \times N$ (N = Avogadro's number).

2.3. Analysis

ESR spectra were recorded at the X-band using a Bruker EMX-10/12 spectrometer (magnetic field modulation: 100 kHz; microwave power level: 1.0 mW) [31,32], with the magnetic field calibrated with DPPH. Catalyst (10 mg) was placed in a quartz tube and treated with 100 Torr oxygen (1 Torr = 133.3 Pa) at 673 K for 1 h. The tube was evacuated at 473 K for 2 h and cooled to room temperature. The required quantity of O_2 or CHA was introduced into the tube. The tube was placed on an ESR sample cavity and photoirradiated at 77 K with a 500 W Xe lamp (USHIO Inc.). After 0.5 h of photoirradiation, measurement was started with continued photoirradiation. The total Cr content of the catalyst was determined by inductively coupled argon plasma atomic emission spectrophotometry (Nippon Jarrell-Ash; ICAP-575 Mark II) after the dissolution of catalyst with HF [33]. BET surface area and pore size distribution of the catalysts were determined by N_2 adsorption–desorption analysis at 77 K using a BELSORP 18PLUS-SP analyzer (BEL Japan, Inc.) [33]. Vapor adsorption analysis with CHA was performed at 298 K using the BELSORP system. DR UV–vis spectra were measured on a UV–vis spectrophotometer (Jasco V-550 with Integrated Sphere Apparatus ISV-469) [34].

3. Results and discussion

3.1. Synthesis and properties of catalysts

Cr-containing MOS catalysts were synthesized with MCM-41 and MOS(x) [x = 5, 10, 20, and 50] supports prepared by a surfactant-templating method. MCM-41 was prepared with TEOS using C_{16}TMABr as a surfactant [29]. The MOS(x) supports were prepared with TEOS and BTESE in the presence of C_{16}TMABr [30]. Powder XRD analysis confirmed that all of these supports showed d_{100} diffraction at 1°–5° (see Supplementary material, Fig. S1). N_2 adsorption–desorption analysis revealed that these supports demonstrated type IV isotherms (see Supplementary material, Fig. S2) and had mesopores 2.6–4.3 nm in diameter. Table 1 (final column) shows the CHA adsorption capacity per unit surface area (q_{CHA}) of the supports, as determined by vapor adsorption measurements with CHA [35]. The q_{CHA} values of MOS(x) (>1.32) were higher than that of MCM-41 (1.06), indicating that the surface hydrophobicity of MOS(x) was actually higher due to the incorporation of ethane fragments [30].

The MOS(x) supports were calcined at 773 K for 4 h under air flow. The resulting MOS(x)-cal supports still contained mesopores 2.9–3.7 nm in diameter (Table 1). The q_{CHA} values of MOS(x)-cal were similar to those of MOS(x), indicating that MOS(x)-cal retained high hydrophobicity even after complete removal of the ethane fragments [30]. During calcination, decomposition of ethane fragments (Si–C cleavage) led to silanol condensation between the resulting Si atom and the adjacent silanol (Si–OH) group, forming a siloxane (Si–O–Si) group [35]. This is confirmed by a decrease in Si–OH absorption (3500 cm^{-1}) on the IR spectra. The silanol condensation led to increased hydrophobicity, thus maintaining the high hydrophobicity.

The Cr-containing catalysts [i.e., Cr/MCM-41, Cr/MOS(x), and Cr/MOS(x)-cal] were synthesized by impregnation of $Cr(NO_3)_3 \cdot 9H_2O$ onto the MCM-41, MOS(x), and MOS(x)-cal supports followed by calcination. All of the catalysts contained mesopores 2.4–3.7 nm in diameter. As shown in Table 2, the q_{CHA} values in Cr/MOS(x) and Cr/MOS(x)-cal were higher than those in Cr/MCM-41, indicating the greater surface hydrophobicity of the former catalysts. The DR UV–vis spectra of the catalysts shown in Fig. 1 (a–i) demonstrate distinctive absorption bands at 350 and 450 nm, assigned to ligand-to-metal charge transfer (LMCT) from O^{2-} to Cr^{6+} transitions of the chromate species, which are highly dispersed on silica matrix [36–39]. In contrast, bulk Cr_2O_3 (j) showed red-shifted absorption at 500–800 nm, assigned to d–d transition of the octahedral Cr^{3+} in Cr_2O_3 cluster. These spectra indicate that

Table 2
Properties of Cr-containing mesoporous silica catalysts

Catalyst	Cr[a] (mol%)	S_{BET}[b] ($m^2\,g^{-1}$)	V_p[c] ($mm^3\,g^{-1}$)	D_p[d] (nm)	a_0[e] (nm)	T_w[f] (nm)	V_m[g] (mmol g^{-1})	q_{CHA}[h] (molecules nm^{-2})
Cr/MCM-41	0.15	925	876	2.4	4.2	2.4	1.59	1.04
Cr/MOS(5)	0.13	881	1283	3.7	5.4	2.6	2.29	1.57
Cr/MOS(10)	0.11	782	1291	3.6	5.5	2.8	2.47	1.90
Cr/MOS(20)	0.18	728	899	3.6	5.5	2.8	1.53	1.27
Cr/MOS(50)	0.12	568	795	3.7	6.3	3.5	1.33	1.41
Cr/MOS(5)-cal	0.14	872	1026	2.9	4.6	2.5	1.91	1.32
Cr/MOS(10)-cal	0.11	809	1268	3.7	3.7	2.1	2.30	1.71
Cr/MOS(20)-cal	0.14	768	859	3.7	5.3	2.4	1.65	1.29
Cr/MOS(50)-cal	0.16	598	843	3.6	6.2	3.6	1.22	1.25

[a] = Cr/(Cr + Si) ×100 (determined by ICP analysis).
[b] BET surface area determined by N_2 adsorption–desorption data (see Supplementary material, Fig. S2).
[c] Pore volume.
[d] Average pore diameter.
[e] Lattice constant determined by XRD (see Supplementary material, Fig. S1).
[f] Wall thickness = $a_0 \times 2/3^{1/2} - D_p$.
[g] Total adsorption capacity of CHA determined by CHA adsorption data (at $p/p_0 = 0.80$).
[h] CHA adsorption capacity per unit surface area = $V_m/10^3 \times 10^{-18}/S_{BET} \times N$ (N = Avogadro's number).

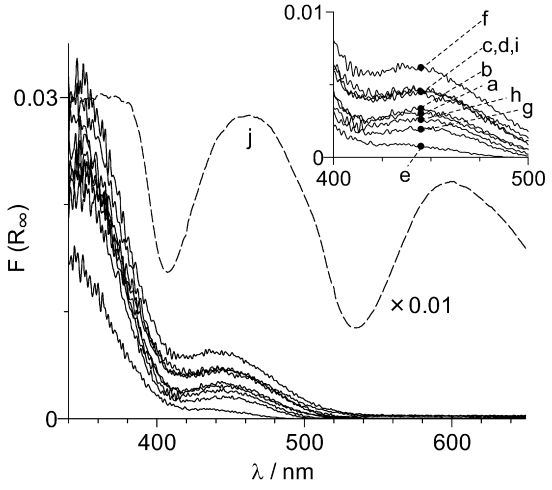

Fig. 1. UV–vis diffuse reflectance spectra of catalysts. (a) Cr/MCM-41, (b) Cr/MOS(5), (c) Cr/MOS(10), (d) Cr/MOS(20), (e) Cr/MOS(50), (f) Cr/MOS(5)-cal, (g) Cr/MOS(10)-cal, (h) Cr/MOS(20)-cal, (i) Cr/MOS(50)-cal, and (j) Cr_2O_3.

Table 3
Results of photocatalytic oxidation of cyclohexane in a solvent free condition[a]

Run	Catalyst	Yield (μmol)			PO product selectivity[b] (%)	TON[c]
		CHA-one	CHA-ol	CO_2		
1	Cr/MCM-41	0.47	0.53	0.33	95	0.8
2	Cr/MOS(5)	0.67	0.72	0.56	94	1.3
3	Cr/MOS(10)	0.46	0.45	0.28	95	1.0
4	Cr/MOS(20)	0.33	0.33	0.63	86	0.4
5	Cr/MOS(50)	Trace	Trace	0.50		
6	Cr/MOS(5)-cal	0.71	0.77	0.70	93	1.3
7	Cr/MOS(10)-cal	1.20	1.06	0.72	95	2.4
8	Cr/MOS(20)-cal	0.48	0.62	0.69	91	0.9
9	Cr/MOS(50)-cal	0.57	0.83	0.77	92	1.1
10	Cr_2O_3	N.D.	N.D.	N.D.		
11	Cr/MCM-41[d]	4.20	1.90	1.00	97	4.9
12	TiO_2 (P25)[e]	11.1	2.20	101	43	

[a] Conditions: catalyst, 50 mg; CHA, 10 ml; O_2, 1 atm; photoirradiation time, 5 h (>400 nm).
[b] = [(PO products)/(PO products + (1/6)CO_2) × 100] (Ref. [6]).
[c] = [(PO product yields)/(Cr amount on the catalyst).
[d] MeCN, 9 ml; CHA, 1 ml.
[e] Catalyst, 10 mg.

Cr/MOS(x) and Cr/MOS(x)-cal contained highly dispersed chromate species.

3.2. Photooxidation selectivity

Photocatalytic CHA oxidation was carried out using Cr/MCM-41, Cr/MOS(x), and Cr/MOS(x)-cal catalysts with O_2 under solvent-free conditions. Table 3 summarizes the yields of CO_2 and PO products (CHA-one and CHA-ol) obtained by >400 nm irradiation with a Xe lamp for 5 h. As shown in runs 1–9, all of the Cr-containing catalysts promoted CHA oxidation. In these cases, no reaction occurred without photoirradiation. As shown in run 10, Cr_2O_3 did not promote oxidation, indicating that polymerized Cr^{3+} was inactive and that the highly dispersed chromate species were the active species [18,19]. In run 11, CHA oxidation on Cr/MCM-41 with acetonitrile solvent showed high PO product selectivity (97%). Even without acetonitrile (runs 1–9), Cr-containing catalysts showed high selectivity (>86%), indicating that neither high surface hydrophobicity of the catalyst nor the absence of solvent affected PO product selectivity. In run 12, TiO_2 (P25), a representative photocatalyst, showed very low selectivity (43%), suggesting that these Cr-containing catalysts were effective in partial CHA oxidation.

3.3. Photocatalytic activity of Cr/MOS(x)-cal catalysts

Fig. 2 shows the TONs for PO product formation during photoirradiation (5 h) on the respective catalysts. As indicated by the gray bar ($x = 0$), Cr/MCM-41 showed very low TON (0.8). In contrast, the TON values of Cr/MOS(x)-cal (white bar) were higher than that of Cr/MCM-41, with Cr/MOS(10)-

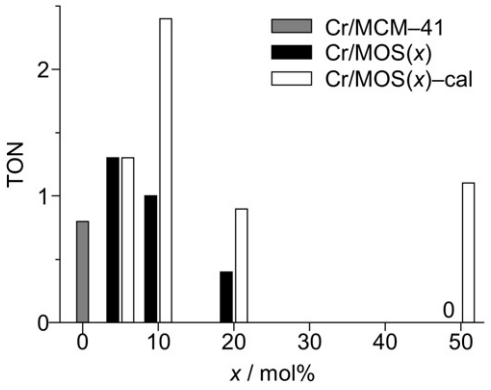

Fig. 2. TON values for PO products formation (= [(PO product yields)/(Cr amount on the catalyst)]) during photoirradiation ($\lambda > 400$ nm, 5 h) of neat CHA with (gray) Cr/MCM-41, (black) Cr/MOS(x), and (white) Cr/MOS(x)-cal catalysts.

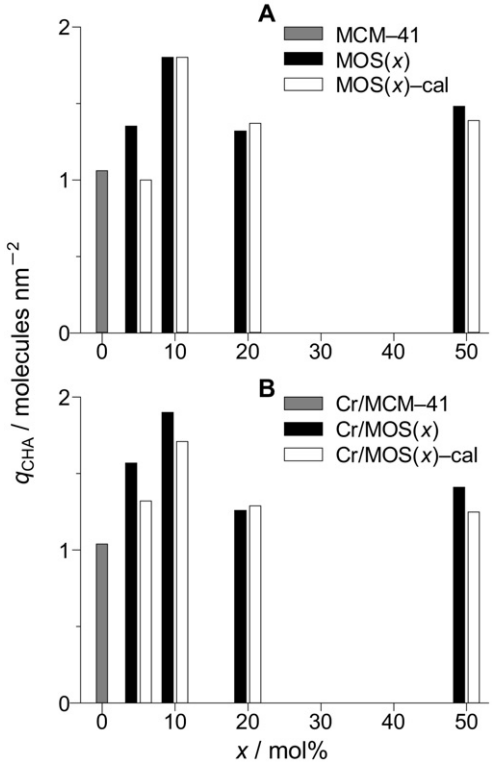

Fig. 3. Adsorption capacity of CHA per unit surface area (q_{CHA}) of (A) supports (MCM-41, MOS(x), and MOS(x)-cal) and (B) catalysts (Cr/MCM-41, Cr/MOS(x), and Cr/MOS(x)-cal).

cal showing threefold higher TON (2.4). The greater activity of Cr/MOS(x)-cal is due to the enhanced access of CHA to the photoexcited chromate species on the hydrophobic surface. As shown in Fig. 3B (white bar), q_{CHA} values were higher in Cr/MOS(5)-cal and Cr/MOS(10)-cal compared with Cr/MCM-41 (gray bar). This indicates that a larger quantity of CHA was adsorbed on the hydrophobic catalyst surface; in other words, the chromate species were surrounded by greater quantities of CHA, accelerating CHA oxidation. After the reaction with Cr/MOS(10)-cal (run 7, Table 3), the catalyst was recovered by filtration and washed with acetonitrile. No leaching of Cr during reaction was detected. In addition, after being reused for further CHA oxidation, the catalyst demonstrated the same PO product selectivity and activity as the virgin catalyst. As shown in Fig. 2 (white bar), the TON values of Cr/MOS(20)-cal and Cr/MOS(50)-cal were much lower than that of Cr/MOS(10)-cal. As shown in Fig. 3B (white bar), the q_{CHA} values of Cr/MOS(20)-cal and Cr/MOS(50)-cal also were much lower than that of Cr/MOS(10)-cal, indicating suppressed access of CHA to the chromate species on these catalysts.

The low q_{CHA} values of Cr/MOS(20)-cal and Cr/MOS(50)-cal are due to the inherent properties of mesopores affected by the amount of BTESE. As shown in Table 1, the average pore diameter (D_p) of MCM-41 and MOS(x) supports increased with increasing amounts of BTESE, with a D_p of 2.6 nm for MCM-41 and 4.3 nm for MOS(50). As shown in Fig. 4 (gray and black circles), the pore size of these supports actually increased with increasing amounts of BTESE. As reported previously [40,41], the multilayer adsorption of molecules decreased with increasing pore size. As shown in Fig. 3A (black bar), the q_{CHA} values of MOS(20) and MOS(50) were much lower than that of MOS(10), indicating that a smaller amount of CHA was actually adsorbed within larger pores. As shown in Fig. 4 (white square), the Cr/MOS(x)-cal with a greater amount of BTESE had a larger pore size, indicating that Cr/MOS(x)-cal derived from MOS(x) with a greater amount of BTESE retained a larger pore size. Thus, the low q_{CHA} values for Cr/MOS(20)-cal and Cr/MOS(50)-cal (Fig. 3B, white bar) are due to their large mesopores, resulting in low catalytic activity (Fig. 2).

3.4. Photocatalytic activity of Cr/MOS(x) catalysts

Fig. 2 (black bar) shows the TONs of the Cr/MOS(x) catalysts synthesized by Cr impregnation onto MOS(x) followed by calcination. The TON of Cr/MOS(5) was higher than that of Cr/MCM-41 and similar to that of Cr/MOS(5)-cal. This is due to the increased surface hydrophobicity; the q_{CHA} of Cr/MOS(5) was actually higher than that of Cr/MCM-41 (Fig. 3B). However, as shown in Fig. 2 (black bar), the TON of Cr/MOS(x) prepared with >10% BTESE was much lower than that of Cr/MOS(x)-cal (white bar). In addition, the TON values decreased with increasing BTESE content. As shown in Fig. 3B (black bar), the q_{CHA} value of Cr/MOS(x) was similar to that of the corresponding Cr/MOS(x)-cal (white bar), indicating that similar amounts of CHA were adsorbed within the mesopores of these catalysts.

The much lower activity of Cr/MOS(x) was due to the collapse of mesopores by calcination, which suppressed the access of CHA to the chromate species. As shown in Fig. 5A, MOS(x) (black bar) had a smaller surface area than MCM-41 (gray bar), independent of the BTESE content. As shown in Fig. 5B (black bar), Cr/MOS(x) had a smaller surface area than the corresponding MOS(x) (Fig. 5A, black bar), due to the removal of ethane fragments by calcination, which led to the condensation of silanol and the collapse of mesopores. As shown in Fig. 4, Cr/MOS(x) (black square) had a much broader pore size distribution than MOS(x) (black circle), indicating that calcination of MOS(x) actually destroyed the mesopores. As shown

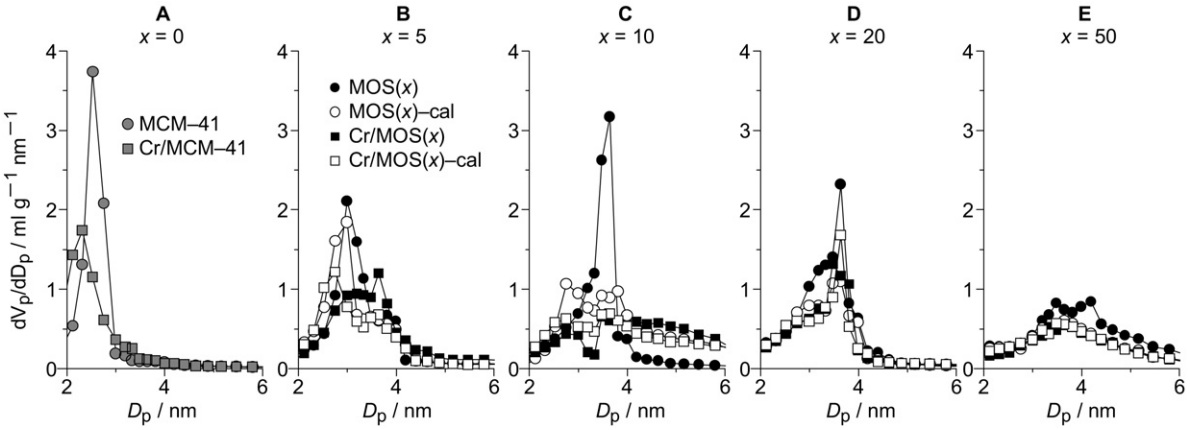

Fig. 4. Pore size distribution of the respective supports and catalysts (MCM-41, Cr/MCM-41, MOS(x), MOS(x)-cal, Cr/MOS(x), and Cr/MOS(x)-cal). (A) $x = 0$ (MCM-41 and Cr/MCM-41), (B) $x = 5$, (C) $x = 10$, (D) $x = 20$, and (E) $x = 50$.

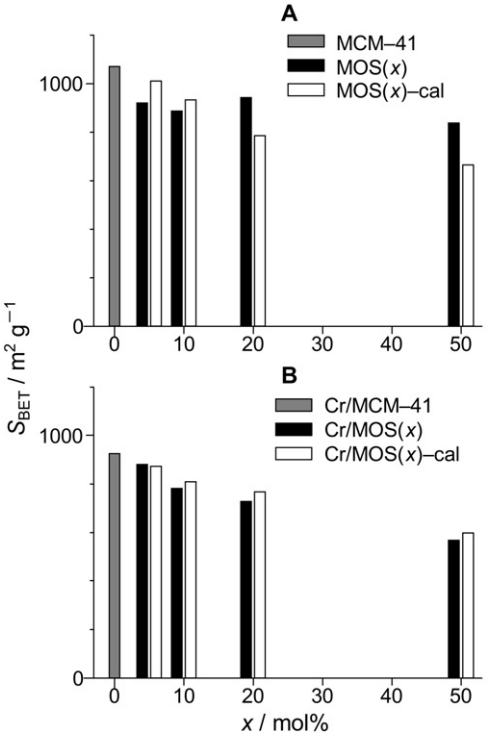

Fig. 5. BET surface area of (A) supports (MCM-41, MOS(x), and MOS(x)-cal) and (B) catalysts (Cr/MCM-41, Cr/MOS(x), and Cr/MOS(x)-cal).

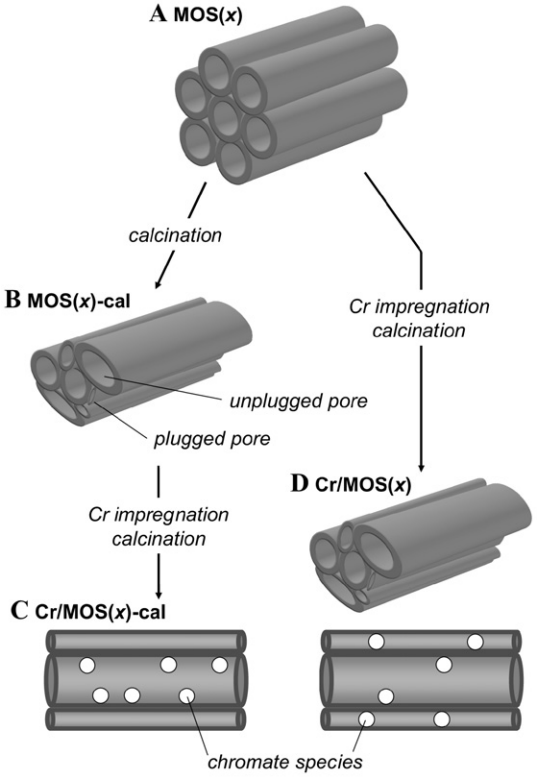

Scheme 1. Schematic representation of pore structure for supports and catalysts.

in Table 1, the pore volume (V_p) of MOS(x) was independent of the BTESE content (1150–1260 $mm^3\ g^{-1}$); however, the V_p's of Cr/MOS(20) and Cr/MOS(50) (Table 2) were low ($<900\ mm^3\ g^{-1}$), indicating that mesopore collapse was more significant on Cr/MOS(x) synthesized with higher BTESE contents.

As shown in Fig. 5, the Cr/MOS(x)-cal had much lower surface area and V_p compared with the corresponding MOS(x). This means that Cr/MOS(x)-cal also contained collapsed pores; however, Cr/MOS(x)-cal demonstrated much higher activity than Cr/MOS(x)(Fig. 2). The difference in activity between Cr/MOS(x) and Cr/MOS(x)-cal is due to the Cr impregnation procedure used (Scheme 1). Cr/MOS(x) was synthesized by impregnation of Cr onto MOS(x) followed by calcination. The calcination led to the collapse of mesopores (pore plugging), blocking access of CHA to the confined chromate species (Scheme 1D) and resulting in very low activity (Fig. 2, black bar). In contrast, Cr/MOS(x)-cal was synthesized by impregnation of Cr onto MOS(x)-cal followed by calcination. The MOS(x)-cal supports also contained plugged pores (Scheme 1B); however, subsequent Cr impregnation led to selective adhesion of Cr species on the unplugged pores, thus allowing access of CHA to the chromate species (Scheme 1C). This is definitely the reason for the activity difference between Cr/MOS(x) and Cr/MOS(x)-cal. The pore-plugging was more significant on the Cr/MOS(x) synthesized with the higher

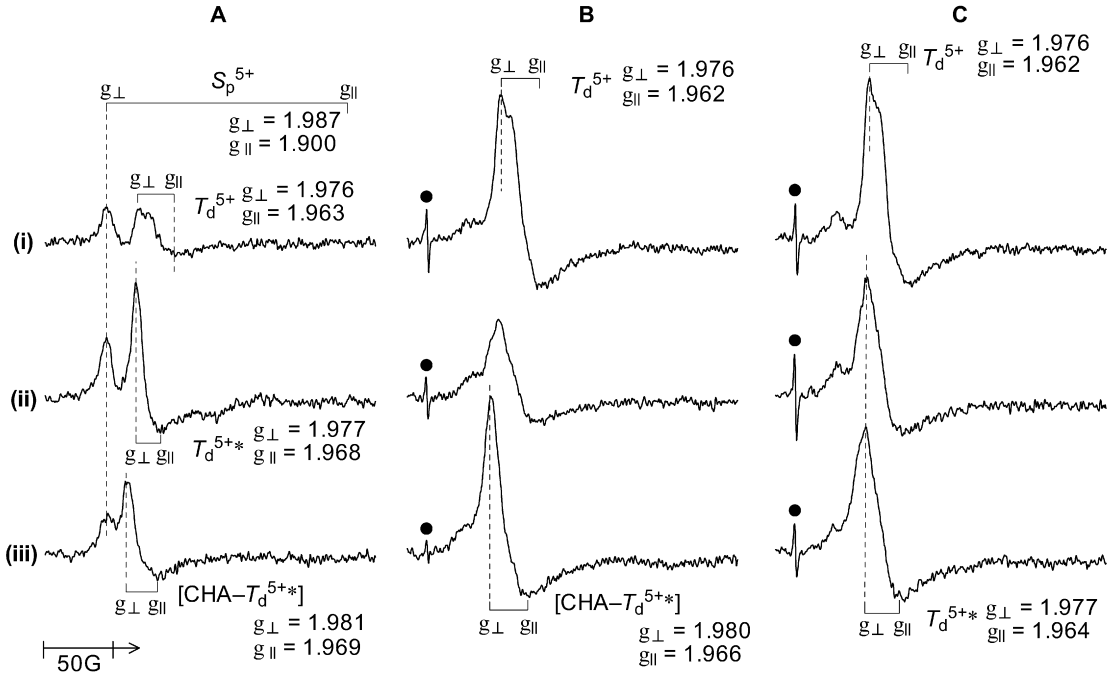

Fig. 6. ESR spectra (77 K) of (A) Cr/MCM-41, (B) Cr/MOS(10)-cal, and (C) Cr/MOS(10) catalysts, when measured (i) in vacuo without photoirradiation, (ii) in vacuo with photoirradiation, and (iii) with photoirradiation in the presence of 1 Torr CHA. The signal indicated by closed circle symbol ($g = 2.003$) is assigned to carbonaceous residues derived from BTESE.

BTESE content, resulting in decreasing activity with increasing BTESE content (Fig. 2, black bar).

3.5. Properties of photoexcited chromate species

Our results reveal that Cr/MOS(x)-cal exhibited high catalytic activity, with Cr/MOS(10)-cal, with high CHA adsorption capacity, showing the greatest catalytic activity. As shown in Fig. 3B, the q_{CHA} of Cr/MOS(10)-cal (white bar) was 1.5-fold higher than that of Cr/MCM-41 (gray bar). However, as shown in Fig. 2, the TON of Cr/MOS(10)-cal (white bar) is 3-fold higher than that of Cr/MCM-41 (gray bar).

As reported previously [18,19], the catalytic activity of chromate species depends on its structure. Consequently, we studied the structure and properties of chromate species on Cr/MOS(10)-cal by ESR analysis and compared them with those of Cr/MCM-41. Chromate species on silica form a tetrahedral (T_d^{6+}) or square-pyramidal (S_p^{6+}) structure [36,37]. Fig. 6A.i shows an ESR spectrum of Cr/MCM-41 measured in vacuo at 77 K. The spectrum comprises two signals assigned to the reduced T_d^{5+} ($g_\perp = 1.976$, $g_{||} = 1.963$) and S_p^{5+} ($g_\perp = 1.987$, $g_{||} = 1.900$) species [36], indicating that both T_d^{6+} and S_p^{6+} species exist on Cr/MCM-41. As shown in Fig. 6A.ii, on photoirradiation to Cr/MCM-41, the T_d^{5+} signal disappeared and a new signal appeared ($g_\perp = 1.977$, $g_{||} = 1.968$), which is assigned to the excited-state T_d^{5+*} species formed by a photo-induced charge transfer between Cr and terminal oxygen (O_T) [42–45]. The T_d^{5+*} formation also was observed on a Cr/SiO_2 catalyst synthesized by Cr impregnation onto amorphous silica [18,19]. In contrast, the S_p^{5+} signal hardly changed, because S_p^{6+} does not form an excited state [18], indicating that on Cr/MCM-41, T_d^{5+*} was acting as the active species for CHA oxidation.

Fig. 6B.i shows an ESR spectrum of Cr/MOS(10)-cal measured in vacuo at 77 K. A strong T_d^{5+} signal can be seen, whereas S_p^{5+} scarcely appears because of T_d^{5+} signal overlap. As shown in Fig. 6B.ii, photoirradiation to Cr/MOS(10)-cal led to formation of a T_d^{5+*} signal, as also occurred for Cr/MCM-41 (Fig. 6A, i and ii). However, the intensity of the T_d^{5+*} signal was lower for Cr/MOS(10)-cal than for Cr/MCM-41, indicating that the T_d^{5+} on Cr/MOS(10)-cal was photoreduced to a species of lower oxidation number (i.e., Cr^{4+}, Cr^{3+}, or Cr^{2+}) [46]. The Cr^{3+} signal does not appear in this spectrum [36]. It is well known that Cr^{2+} is readily oxidized by O_2 to Cr^{3+} [36]; however, photoirradiation to Cr/MOS(10)-cal with O_2 demonstrated no Cr^{3+} signal. These findings imply that Cr^{4+} is involved in the excited T_d species and thus T_d^{4+*} species may form on the Cr/MOS(10)-cal catalyst. T_d^{4+*} formation also has been observed on a Cr-SiO_2 catalyst synthesized by a sol–gel method with TEOS and $Cr(NO_3)_3$ [18,19].

The differences in the excited-state T_d species in Cr/MCM-41 (T_d^{5+*}) and Cr/MOS(10)-cal (T_d^{4+*}) are related to the surface conditions of the supports (Scheme 2). In Cr/MCM-41, Cr species were impregnated on a "flat" surface of MCM-41, resulting in a formation of "upright" T_d^{6+} species (Scheme 2A.a) [42,44], as was the case for Cr/SiO_2 synthesized with Cr impregnation on amorphous silica [18,19]. In contrast, in Cr/MOS(10)-cal, Cr species were impregnated on MOS(10)-cal support prepared by calcination of MOS(10). Calcination of MOS(10) led to the removal of ethane fragments; thus, the resulting MOS(10)-cal had a "rough" silica surface. Consequently, impregnation of Cr onto MOS(10)-cal created

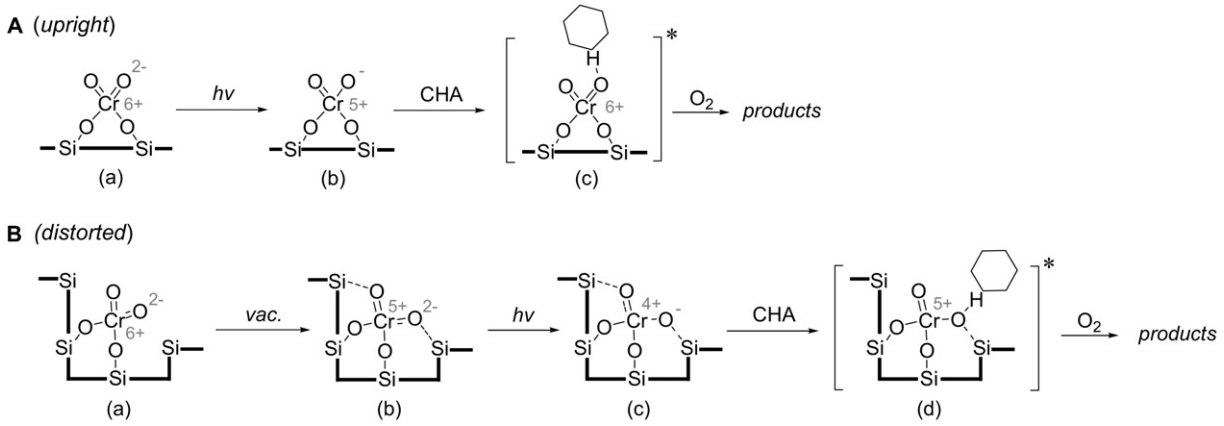

Scheme 2. Photocatalytic mechanism on (A) upright T_d^{6+} species and (B) distorted T_d^{6+} species.

T_d^{6+} with a "distorted" structure (Scheme 2B.a). As shown in Fig. 6B.i, the T_d^{5+} signal intensity on Cr/MOS(10)-cal obtained in vacuo without photoirradiation was much stronger than that on Cr/MCM-41 (Fig. 6A.i). The reduction of Cr^{6+} to Cr^{5+} occurs through formation of the terminal oxygen (O_T)–Si bond, associated with a removal of H_2O from the adjacent Si species [37]. The O_T–Si bond formed more easily on Cr/MOS(10)-cal with the distorted T_d^{6+} than on Cr/MCM-41 with the upright T_d^{6+} (Scheme 2B.b), resulting in strong T_d^{5+} signal intensity (Fig. 6B.i). On the stabilized T_d^{5+}, photoinduced charge transfer between O_T and Cr occurred more readily, promoting T_d^{4+*} formation (Scheme 2B.c). In contrast, on the upright T_d^{6+} on Cr/MCM-41, O_T–Si bond formation hardly occurred, thus forming T_d^{5+*} (Fig. 6A.ii; Scheme 2A.b) [42].

The much higher activity of Cr/MOS(10)-cal compared with Cr/MCM-41 (Fig. 2) is due to the difference in activity between T_d^{4+*} and T_d^{5+*}. Photoirradiation to both catalysts with O_2 at 77 K showed no ESR signals assigned to oxygen radicals ($O_2^-\cdot$, $O_3^-\cdot$) [47,48], indicating that oxygen radicals are not involved in these systems. Fig. 6B.iii shows an ESR spectrum of Cr/MOS(10)-cal obtained by photoirradiation with CHA (1 Torr) at 77 K, demonstrating a new T_d^{5+*} signal ($g_\perp = 1.980$; $g_{||} = 1.966$). The O_T^-, formed by photoinduced charge transfer (Schemes 2A.b and 2B.c), has an electrophilic character [49] and thus acts as a positive hole [50]. The new signal can be assigned to a [CHA–T_d^{5+*}] complex formed via attraction of the CHA proton by the electrophilic O_T^- on T_d^{4+*} (Scheme 2B.d), where Cr^{4+} is oxidized to Cr^{5+} [18,19]. Thus, CHA oxidation on Cr/MOS(10)-cal proceeds through a reaction of the [CHA–T_d^{5+*}] complex with O_2 [18,19]. In contrast, photoirradiation to Cr/MCM-41 with CHA demonstrated a very small [CHA–T_d^{5+*}] signal (Fig. 6A.iii), because T_d^{4+*} hardly formed. The T_d^{5+*} formed on Cr/MCM-41 produced a [CHA–T_d^{6+*}] complex via attraction of CHA protons along with oxidation of Cr^{5+} to Cr^{6+} (Scheme 2A.c) [19]. CHA oxidation on Cr/MCM-41 proceeds via a reaction of the [CHA–T_d^{6+*}] complex with O_2 [19]. The O_T^- adjacent to highly reduced Cr^{4+} has greater electrophilicity than the O_T^- adjacent to Cr^{5+}. Thus, the attraction of CHA proton by the more electrophilic O_T^- on Cr/MOS(10)-cal is stronger than that on Cr/MCM-41, resulting in higher CHA oxidation activity. This is the likely reason for the much higher activity of Cr/MOS(10)-cal compared with Cr/MCM-41 (Fig. 2).

3.6. Access of CHA to photoexcited chromate species

As shown in Fig. 2, Cr/MOS(10) demonstrated much lower activity than Cr/MOS(10)-cal, even though the two catalysts had similar q_{CHA} values (Fig. 3B). This finding implies that the lower activity of Cr/MOS(10) is due to the plugging of mesopores by calcination, which suppresses access of CHA to the chromate species (Scheme 1D). This was confirmed by the ESR spectra of Cr/MOS(10) (Fig. 6C). The spectra obtained in vacuo without and with photoirradiation are similar to those of Cr/MOS(10)-cal (Fig. 6B), indicating that T_d^{4+*} species also form by photoirradiation on Cr/MOS(10), because T_d^{6+} has a distorted structure on the rough surface formed by calcination (Scheme 2B.a). As shown in Fig. 6B.iii, photoirradiation to Cr/MOS(10)-cal with CHA produced a [CHA–T_d^{5+*}] signal; however, as shown in Fig. 6C.iii, photoirradiation to Cr/MOS(10) with CHA did not produce this signal, with the T_d^{5+*} signal remaining even in the presence of CHA. This means that the attraction of the CHA protons by T_d species does not occur on Cr/MOS(10), because the T_d species exist within the plugged pores and thus suppress access of CHA to the species. These findings fully support our assumption (Scheme 1D). In contrast, on Cr/MOS(10)-cal, Cr species were impregnated selectively on the unplugged pores (Scheme 1C), allowing access of CHA access to T_d^{4+*} and resulting in high catalytic activity (Fig. 2).

4. Conclusion

In this work, Cr-containing mesoporous silica catalysts (Cr/MOS and Cr/MOS-cal) with highly dispersed chromate species were synthesized by impregnation of Cr onto MOS supports prepared with TEOS and BTESE. Cr/MOS was synthesized by impregnation of Cr onto MOS followed by calcination. In contrast, Cr/MOS-cal was synthesized by calcination of MOS, impregnation of Cr, and calcination. These

steps were used for neat CHA oxidation with O_2 under visible light. Both catalysts demonstrated higher surface hydrophobicity compared with Cr/MCM-41 prepared only with TEOS. Both promoted partial CHA oxidation with high selectivity. Cr/MOS-cal showed higher activity than Cr/MCM-41, with Cr/MOS(10)-cal synthesized with 10% BTESE exhibiting the highest activity. This is due mainly to the increased surface hydrophobicity, which enhances access of CHA to the chromate species. Cr/MOS demonstrated very low photocatalytic activity due to the plugging of mesopores by calcination, which suppressed access of CHA to the chromate species. Photoactivation of tetrahedrally coordinated chromate species (T_d^{6+}) on Cr/MOS(10)-cal led to the formation of excited-state T_d^{4+*} species. The T_d^{4+*} was found to strongly attract CHA protons due to high electrophilicity, thereby promoting efficient CHA oxidation. This mechanism also contributes to the high catalytic activity of Cr/MOS(10)-cal.

Acknowledgments

This work was supported by a Grant-in-Aid for Scientific Research (19760536) from the Ministry of Education, Culture, Sports, Science and Technology, Japan (MEXT). The authors thank the Division of Chemical Engineering for use of the Lend-Lease Laboratory System.

Supplementary material

The online version of this article contains powder XRD patterns (Fig. S1) and N_2 adsorption–desorption isotherms (Fig. S2) of the supports and catalysts.

Please visit DOI: 10.1016/j.jcat.2008.01.016.

References

[1] U. Schuchardt, D. Cardoso, R. Sercheli, R. Pereira, R.S. da Cruz, M.C. Guerreiro, D. Mandelli, E.V. Spinacé, E.L. Pires, Appl. Catal. A 211 (2001) 1.
[2] G. Bellussi, C. Perego, Cattech 4 (2000) 4.
[3] R. Zhao, D. Ji, G. Lv, G. Qian, L. Yan, X. Wang, J. Suo, Chem. Commun. (2004) 904.
[4] R. Raja, G. Sankar, J.M. Thomas, J. Am. Chem. Soc. 121 (1999) 11926.
[5] C. Giannotti, S. Le Greneur, O. Watts, Tetrahedron Lett. 24 (1983) 5071.
[6] G. Lu, H. Gao, J. Suo, S. Li, J. Chem. Soc. Chem. Commun. (1994) 2423.
[7] P. Boarini, V. Carassiti, A. Maldotti, R. Amadelli, Langmuir 14 (1998) 2080.
[8] A. Sclafani, J.M. Herrmann, J. Phys. Chem. 100 (1996) 13655.
[9] K.-I. Shimizu, T. Kaneko, T. Fujishima, T. Kodama, H. Yoshida, Y. Kitayama, Appl. Catal. A 225 (2002) 185.
[10] C.B. Almquist, P. Biswas, Appl. Catal. A 214 (2001) 259.
[11] M.A. Brusa, M.A. Grela, J. Phys. Chem. B 109 (2005) 1914.
[12] M.A. Gonzalez, S.G. Howell, S.K. Sikdar, J. Catal. 183 (1999) 159.
[13] R. Amadelli, M. Bregola, E. Polo, V. Carassiti, A. Maldotti, J. Chem. Soc. Chem. Commun. (1992) 1355.
[14] A. Molinari, R. Amadelli, L. Antolini, A. Maldotti, P. Battioni, D. Mansuy, J. Mol. Catal. A 158 (2000) 521.
[15] A. Maldotti, A. Molinari, G. Varani, M. Lenarda, L. Storaro, F. Bigi, R. Maggi, A. Mazzacani, G. Sartori, J. Catal. 209 (2002) 210.
[16] K. Teramura, T. Tanaka, T. Yamamoto, T. Funabiki, J. Mol. Catal. A 165 (2001) 299.
[17] K. Teramura, T. Tanaka, M. Kani, T. Hosokawa, T. Funabiki, J. Mol. Catal. A 208 (2004) 299.
[18] Y. Shiraishi, Y. Teshima, T. Hirai, Chem. Commun. (2005) 4569.
[19] Y. Shiraishi, Y. Teshima, T. Hirai, J. Phys. Chem. B 110 (2006) 6257.
[20] A. Corma, P. Esteve, A. Martínez, J. Catal. 161 (1996) 11.
[21] T. Blasco, M.A. Camblor, A. Corma, P. Esteve, J.M. Guil, A. Martínez, J.A. Perdigón-Melón, S. Valencia, J. Phys. Chem. B 102 (1998) 75.
[22] T. Blasco, A. Corma, M.T. Navarro, J.P. Pariente, J. Catal. 156 (1995) 65.
[23] K.A. Koyano, T. Tatsumi, Y. Tanaka, S. Nakata, J. Phys. Chem. B 101 (1997) 9436.
[24] T. Tatsumi, K.A. Koyano, N. Igarashi, Chem. Commun. (1998) 325.
[25] T. Asefa, M.J. MacLachlan, N. Coombs, G.A. Ozin, Nature 402 (1999) 867.
[26] S. Inagaki, S. Guan, Y. Fukushima, T. Ohsuna, O. Terasaki, J. Am. Chem. Soc. 121 (1999) 9611.
[27] A. Corma, J.L. Jordá, M.T. Navarro, F. Rey, Chem. Commun. (1998) 1899.
[28] M.P. Kapoor, A. Bhaumik, S. Inagaki, K. Kuraoka, T. Yazawa, J. Mater. Chem. 12 (2002) 3078.
[29] K.A. Koyano, T. Tatumi, Microporous Mater. 10 (1997) 259.
[30] A. Bhaumik, M.P. Kapoor, S. Inagaki, Chem. Commun. (2003) 470.
[31] Y. Shiraishi, N. Saito, T. Hirai, J. Am. Chem. Soc. 127 (2005) 8304.
[32] H. Koizumi, Y. Shiraishi, S. Tojo, M. Fujitsuka, T. Majima, T. Hirai, J. Am. Chem. Soc. 128 (2006) 8751.
[33] Y. Shiraishi, M. Morishita, Y. Teshima, T. Hirai, J. Phys. Chem. B 110 (2006) 6587.
[34] Y. Shiraishi, N. Saito, T. Hirai, Chem. Commun. (2006) 773.
[35] M. Morishita, Y. Shiraishi, T. Hirai, J. Phys. Chem. B 110 (2006) 17898.
[36] B.M. Weckhuysen, I.E. Wachs, R.A. Schoonheydt, Chem. Rev. 96 (1996) 3327.
[37] B.M. Weckhuysen, A.A. Verberckmoes, A.L. Buttiens, R.A. Schoonheydt, J. Phys. Chem. 98 (1994) 579.
[38] T. Kamegawa, J. Morishima, M. Matsuoka, J.M. Thomas, M. Anpo, J. Phys. Chem. C 111 (2007) 1076.
[39] F. Amano, T. Yamaguchi, T. Tanaka, J. Phys. Chem. B 110 (2006) 281.
[40] Y. Long, T. Xu, Y. Sun, W. Dong, Langmuir 14 (1998) 6173.
[41] H.Y. Zhu, L.A. Ni, G.Q. Lu, Langmuir 15 (1999) 3632.
[42] H. Yamashita, S. Ohshiro, K. Kida, K. Yoshizawa, M. Anpo, Res. Chem. Intermed. 29 (2003) 881.
[43] H. Yamashita, K. Yoshizawa, M. Ariyuki, S. Higashimoto, M. Che, M. Anpo, Chem. Commun. (2001) 435.
[44] M. Matsuoka, M. Anpo, J. Photochem. Photobiol. C 3 (2003) 225.
[45] S. Rodorigues, K.T. Ranjit, S. Uma, I.N. Martyanov, K.J. Klabunde, J. Catal. 230 (2005) 158.
[46] B.M. Weckhuysen, R.A. Schoonheydt, J.-M. Jehng, I.E. Wachs, S.J. Cho, R. Ryoo, S. Kljlstra, E. Poels, J. Chem. Soc. Faraday Trans. 91 (1995) 3245.
[47] Y. Shiraishi, N. Saito, T. Hirai, J. Am. Chem. Soc. 127 (2005) 12820.
[48] Y. Shiraishi, M. Morishita, T. Hirai, Chem. Commun. (2005) 5977.
[49] H. Koizumi, T. Takada, T. Ichikawa, A. Lund, Chem. Phys. Lett. 340 (2001) 256.
[50] K. Wada, H. Yamada, Y. Watanabe, T. Mitsudo, J. Chem. Soc. Faraday Trans. 94 (1998) 1771.